ACS APPLIED MATERIALS & INTERFACES

www.acsami.org

Research Article

Exosome-like Nanovesicles Derived from the Mucilage of *Pinctada Martensii* Exhibit Antitumor Activity against 143B Osteosarcoma Cells

Peng Li, Lihua Ma, Weiqiang Zhan, Dong Xie, Guanhao Hong, Mingzhu Deng, Zijie Wu, Peichun Lin, Linhong Yan, Zifan Lu, Chengyong Li,* and Hao Lin*

Cite This: *ACS Appl. Mater. Interfaces* 2023, 15, 26227−26240

Read Online

ACCESS | Metrics & More | Article Recommendations | Supporting Information

ABSTRACT: Osteosarcoma is prone to metastasis and has a low long-term survival rate. The drug treatment of osteosarcoma, side effects of treatment drugs, and prognosis of patients with lung metastasis continue to present significant challenges, and the efficacy of drugs used in the treatment of osteosarcoma remains low. The development of new therapeutic drugs is urgently needed. In this study, we successfully isolated *Pinctada martensii* mucilage exosome-like nanovesicles (PMMENs). Our findings demonstrated that PMMENs inhibited the viability and proliferation of 143B cells, induced apoptosis, and inhibited cell proliferation by suppressing the activation of the ERK1/2 and Wnt signaling pathways. Furthermore, PMMENs inhibited cell migration and invasion by downregulating N-cadherin, vimentin, and matrix metalloprotease-2 protein expression levels. Transcriptomic and metabolomic analyses revealed that differential genes were co-enriched with differential metabolites in cancer signaling pathways. These results suggest that PMMENs may exert anti-tumor activity by targeting the ERK1/2 and Wnt signaling pathways. Moreover, tumor xenograft model experiments showed that PMMENs can inhibit the growth of osteosarcoma in mice. Thus, PMMENs may be a potential anti-osteosarcoma drug.

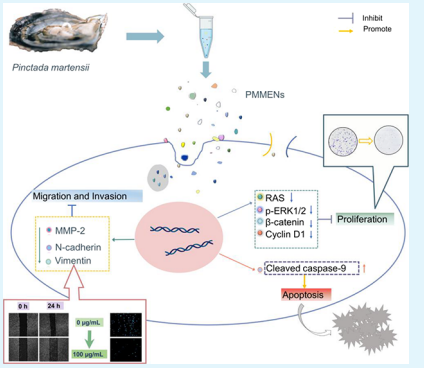

KEYWORDS: *Pinctada martensii, exosome-like nanovesicles, osteosarcoma, proliferation, ERK1/2, Wnt/β-catenin signaling*

1. INTRODUCTION

Osteosarcoma is the most prevalent bone malignancy, mainly affecting adolescents or children under the age of 20, and the third most common cancer in this population.[1,2] The incidence of osteosarcoma peaks during adolescence and at approximately 60 years of age. At diagnosis, osteosarcoma metastasizes globally in approximately 20% of patients, with the lung being the most common site of metastasis, accounting for 90% of cases.[3−5] Currently, the primary treatment for osteosarcoma is a combination of preoperative adjuvant chemotherapy, surgical resection, and postoperative adjuvant chemotherapy, which has increased the 10-year patient survival rate from 30 to 50%. However, the 5-year and overall survival rates of patients with osteosarcoma have not increased and plateaued, and osteosarcoma relapses in 30−40% of patients within 1−2 years after surgery. The prognosis for relapsed patients is poor, with only 23−29% of patients surviving over five years after the second diagnosis,[2] and the long-term survival rate after relapse is less than 20%.[6,7] To improve the survival rates of patients with osteosarcoma, multi-drug adjuvant chemotherapy regimens with doxorubicin, cisplatin, high-dose methotrexate, and ifosfamide as antagonists are used.[1] However, high chemotherapy doses may cause severe and life-threatening toxicity.[5,6,8,9] Therefore, the development of novel low-toxic and biocompatible agents for treating osteosarcoma is urgently required.

Extracellular vesicles (EVs), which are natural, cell-derived vesicles composed of phospholipid bilayers, are divided into three major subtypes: microvesicles, exosomes, and apoptotic bodies.[10] EVs encapsulate cell-derived contents and mediate intercellular communication through local and distant transport of functional substances, including RNA, DNA, proteins, and lipids.[11] They can function as biomarkers, therapeutic agents, and drug carriers.[12] EVs play a crucial role in intercellular communication, signal transduction, and tumor metastasis,[13,14] and several studies have focused on using EVs to treat diseases such as cancer,[15,16] inflammatory diseases,[17] neurological disorders,[18] myocardial infarction,[19] and stroke.[20] EVs have great potential as drugs for treating diseases. *Momordica charantia*-derived EV-like nanovesicles isolated from bitter melon juice exhibited anti-tumor activity against

Received: November 29, 2022
Accepted: May 15, 2023
Published: May 25, 2023

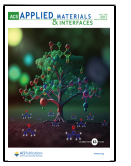

U251 glioma cells and protected cardiomyocytes from radiation damage by attenuating DNA damage and mitochondrial dysfunction.[21,22] Yang et al. found that lemon-derived EVs induced reactive oxygen species production in gastric cancer cells, thus exerting anti-cancer effects.[23] EVs have diverse origins and have been isolated from mammalian cells (such as mesenchymal stem cells and epithelial cells), biological fluids (such as blood, urine, and saliva),[24] plants and fruits (such as grapes, grapefruit, broccoli, and blueberries),[17,25−27] and marine organisms.[28]

Marine biological resources have recently been considered an alternative source of biological materials for terrestrial vertebrates. The metabolism of marine organisms produces substances with anti-inflammatory, anti-cancer, antioxidant, and pro-wound healing physiological activities. The pearl oyster *Pinctada martensii*, an economically important marine bivalve, is the primary marine shellfish cultured for pearl production in southern China. With the success of fisheries and artificial pearl production culture, the annual *P. martensii* meat yield (all organs) from Hepu, Guangxi Province, is 2000−3000 tons.[29] In addition to its use in pearl and raw food production, bioactive substances with anti-tumor, anti-fatigue, antioxidant,[29] wound healing,[30] and antibacterial[31] properties, such as taurine, zinc, active peptides, and C-type lectins, have been extracted from *P. martensii*. However, there have been relatively few studies on the active constituents of *P. martensii* mucilage and its therapeutic efficacy. Notably, *P. martensii* mucilage is often discarded as a waste liquid during *P. martensii* meat processing, and investigating the possible active substances in this mucilage would greatly contribute to complete resource utilization. Successful isolation of EVs from the mucus of cod[32] and flatfish[33] has been reported. Therefore, we speculate that EVs derived from *P. martensii* mucilage also possess biological activity.

In this study, we successfully isolated *P. martensii* mucilage exosome-like nanovesicles (PMMENs) from *P. martensii* mucilage through ultracentrifugation. PMMENs were characterized and analyzed using transmission electron microscopy and atomic force microscopy. Additionally, we evaluated the effects of PMMENs on the proliferation, migration, invasion, and apoptosis of 143B cells to determine their anti-tumor potential. The findings of this study will serve as a reference for further exploration of *P. martensii* mucilage.

2. EXPERIMENTAL SECTION

2.1. Materials and Reagents. *P. martensii* mucilage was provided by Guangdong Zunding Pearl Co. (Zhanjiang, China). Human osteosarcoma cells (143B cells) were purchased from KeyGEN Biotech (Jiangsu, China). Human Umbilical Vein Endothelial Cells (HUVECs) and human hepatoma cell lines (HepG-2) were purchased from the Cell Bank of the Chinese Academy of Sciences (Shanghai, China). The human gastric adenocarcinoma cell line AGS was obtained from the Shanghai Institute of Biosciences Cell Resource Center, Chinese Academy of Sciences (Shanghai, China). The human osteoblast (hFOB 1.19) was purchased from Shanghai Aoyin Biotechnology (Shanghai, China). Phosphate buffered saline (PBS) was purchased from BI (Kibbutz Beit HaEmek, Israel). Fetal bovine serum (FBS), Dulbecco's modified Eagle medium (DMEM), Ham's F 12 nutrient medium (F12), Dulbecco's Modified Eagle Medium/Nutrient Mixture F-12 (DMEM/F12), penicillin, streptomycin, and 0.25% trypsin−EDTA were purchased from Gibco (New York, NY, USA). Propidium iodide (PI) was purchased from Yessen Biotechnology Co. (Shanghai, China). ActinRed was provided by Kegen Biotechnology Co., Ltd. (Jiangsu, China). Exosome green fluorescent marker stain (PKH67) was purchased from Umibio Biotechnology Co., Ltd. (Shanghai, China). The BCA protein assay kit, lactate dehydrogenase (LDH) cytotoxicity assay kit, 4′,6-diamidino-2-phenylindole (DAPI), Hoechst 33342, and RIPA lysis buffer were obtained from Beyotime Biotechnology (Shanghai, China). The TRIzol reagent kit, HiScript III RT SuperMix for qPCR (+gDNA wiper) for qPCR kit, and ChamQ Universal SYBR qPCR Master Mix kit were purchased from Vazyme (Nanjing, China). Primary antibodies including β-catenin (E-5, sc-7963), cyclin D1 (A-12, sc-8396), N-cadherin (13A9, sc-59,987), vimentin (V9: sc-6260), caspase-9 (9508), cleaved caspase-9 (2075s), CD63 (MX-49.129.5, sc-5275), CD9 (C-4: sc-13,118), and HSP70 (3A3, sc-32,239), ERK1/2 (sc-514,302), β-actin (sc-130,300), and p-ERK1/2 (sc-81,492) were obtained from Santa Cruz Biotechnology Inc. (USA). Primary antibody MMP-2 (D8N9Y) and secondary antibodies: anti-rabbit IgG (7074 S) and anti-mouse IgG (sc-2357) were purchased from Cell Signaling Technology Inc. (USA).

2.2. Cell Culture. 143B and HepG-2 cells were cultured in DMEM supplemented with 10% FBS and 1% penicillin−streptomycin under standard cell culture conditions. The AGS and hFOB 1.19 cells were cultured in F12 and DMEM/F12 medium containing 10% FBS and 1% penicillin−streptomycin, respectively. All cells were cultured under sterile conditions in a humidified incubator containing 5% CO_2 at 37 °C.

2.3. Extraction of PMMENs. Freshly collected *P. martensii* mucilage was aliquoted into 500 mL bottles and stored at −80 °C until use. Mucilage was then placed in a 50 mL centrifuge tube and centrifuged at 500 × *g* and 4 °C for 10 min, 2000 × *g* for 10 min, and 10,000 × *g* for 30 min. The supernatant was then placed in a horizontal rotor (P28S, Hitachi Koki, Japan) for the first ultracentrifugation (Himal CP 70NE) at 100,000 × *g* and 4 °C for 70 min. The precipitate was resuspended in pre-chilled PBS, filtered through a 0.22 μm membrane, and then transferred to a new tube for a second ultracentrifugation at 100,000 × *g* and 4 °C for 90 min. The precipitate was resuspended in 200 μL of PBS, transferred to a microcentrifuge tube, and stored at −80 °C. The extracted nanovesicles were quantified using a BCA assay kit (Thermo Scientific).

2.4. Dynamic Light Scattering and Nanoparticle Tracking Analysis. The size distribution of nanovesicles was determined through dynamic light scattering (DLS). PMMENs were collected and diluted 100-fold with PBS to prevent inter-particle interactions. The diluted PMMENs were then placed in the constant temperature cell chamber of a laser particle sizer (Zetasizer Nano ZSE, Malvern, UK) for measurement. The Brownian motion of the PMMENs was dynamically tracked in real-time using nanoparticle tracking analysis (NTA), and their particle size distribution and concentration were determined using ZetaVIEW (Particle Metrix).

2.5. Transmission Electron Microscopy and Atomic Force Microscopy. Briefly, 10 μL of PMMENs were fixed on a copper mesh, stained with 3% phosphotungstic acid, air-dried at 26 °C for 20 min, and observed using transmission electron microscopy (TEM) (JEM-1400). Atomic force microscopy (AFM) images were obtained by adding several drops of well-dispersed PMMENs dropwise on mica sheets, air-drying them, and then capturing images with a Bruker Dimension Icon AFM.

2.6. PMMEN Uptake by 143B Cells. PMMENs were labeled with PKH67 following the manufacturer's instructions. PMMENs were added to the PKH67 dye working solution, mixed for 1 min using a vortex shaker, and then allowed to stand for 10 min. Next, PBS was added to the PMMENs−dye complexes, and PMMENs were re-extracted to remove the excess dye. The resulting precipitate was resuspended in 200 μL of PBS, which represented the stained PMMENs. To analyze the uptake of PMMENs by 143B cells, the cells were plated in confocal dishes, incubated until 70−80% confluent, and further incubated with 50 μg/mL of labeled PMMENs for 24 h. The cytoskeleton and nuclei of the cells were analyzed using ActinRed and DAPI, respectively. Fluorescence images were obtained using a laser confocal microscope (LSCM, Olympus Fv300, Japan).

2.7. Determination of Cell Viability. Cell viability was determined using the Cell Counting Kit-8 (CCK-8) assay according

https://doi.org/10.1021/acsami.2c21485
ACS Appl. Mater. Interfaces 2023, 15, 26227−26240

to the manufacturer's instructions. Briefly, 143B cells were inoculated in 96-well plates at a density of 5000 cells/well and incubated overnight. Then, the complete medium was removed, and the cells were washed with PBS. Different concentrations of PMMENs (0, 0.5, 1, 5, 50, 100, 150, 200, 500 μg/mL) were co-incubated with the cells for 24 h. After incubation, 10 μL of the CCK-8 reagent was added to each well, and the plates were gently shaken and incubated at 37 °C in the dark for 1 h. The absorbance at 450 nm was measured using a microplate reader (Varioskan Flash, USA). HepG-2, HUVEC, AGS, and hFOB 1.19 cells were treated with PMMENs (0, 5, 50, 100, 150, 200, 500 μg/mL), and the cell viability was determined by the same method as that of 143B cells.

2.8. Clonogenic Assay. For the clonogenic assay, 143B cells (1000 cells/well) were inoculated in each well of a 6-well plate and cultured for a week with medium change every 2−3 days. On day 7, the cells were fixed with formaldehyde for 30 min, stained with 1% crystal violet for 10 min, and air-dried at 26 °C; the number of colonies containing over 50 cells was counted.

2.9. LDH Release Rate Determination. Appropriate amounts of cells were inoculated in 96-well cell culture plates to ensure that the cell density did not exceed 80−90% during the assay. The culture medium was then aspirated, and the wells were washed once with PBS. The wells were then divided into the following groups: culture medium with no cells (background blank control wells), control cells without PMMEN treatment (sample control wells), cells without PMMEN treatment for subsequent lysis (sample maximal enzyme activity control wells), and PMMEN-treated cell samples. The plates were placed in the incubator for 24 h and removed from the incubator 1 h before the scheduled assay time point. The LDH release reagent was added to the "sample maximal enzyme activity control wells" at 10% of the original culture volume. The culture was triturated several times and re-placed in the incubator. At the designated time point, the supernatant of each well was centrifuged at 400 × g for 5 min. Then, 120 μL of supernatant from each well was added to the corresponding wells of a new 96-well plate, and the absorbance at 490 nm was measured using a microplate reader.

2.10. Hoechst 33342 and PI Staining. 143B cells were co-incubated with PMMENs at concentrations of 0, 5, 50, or 100 μg/mL for 24 h. The cells were then washed twice with pre-chilled PBS, stained with Hoechst 33342 for 30 min, gently washed with PBS, and stained with PI for 5 min. Fluorescence images were acquired using a laser confocal microscope (LSCM, Olympus Fv300, Japan).

2.11. Wound Healing Assay. Briefly, 143B cells (5×10^5 cells/well) were inoculated into 24-well plates. When the cells reached 100% confluence, a wound (scratch) was artificially created using a 200 μL pipette tip, followed by washing three times with PBS to remove nonadherent cells. Then, the cells were incubated with 0, 5, 50, or 100 μg/mL PMMENs. Wound images were captured at 0 and 24 h under a light microscope and analyzed using ImageJ software. The results were quantified using the following equation:

$$\text{wound healing rate} = \frac{\text{wound area (0 h)} - \text{wound area (24 h)}}{\text{wound area (0 h)}}$$

2.12. Cell Invasion Assay. Cell invasiveness was assessed using 24-well Transwell plates with a pore size of 8 μm (Corning Inc., USA). Briefly, 100 μL of the diluted Matrigel was added to the chamber and incubated for 30 min at 37 °C in an incubator. Then, 100 μL of 143B cell suspension was inoculated into the upper chamber and treated with 0, 5, 50, or 100 μg/mL PMMENs. Next, 600 μL of DMEM containing 10% FBS was added to the lower chamber and incubated at 37 °C and 5% CO_2 for 12 h. The chamber was removed and rinsed three times with PBS. The cells on the upper layer of the microporous membrane were gently wiped off using a cotton swab and stained with an anti-quenching fluorescent dye containing DAPI. Three random fields of view were selected for cell observation using an inverted microscope, and the average value was used as the number of cells that passed through the chamber.

2.13. Protein Immunoblotting. For protein immunoblotting, 143B cells were lysed with RIPA solution containing 1% PMSF (Beyotime, China). Then, the extracted proteins were quantified using a BCA kit (Thermo Fisher, USA). Equal amounts of protein from different groups were separated using 12% sodium dodecyl sulfate-polyacrylamide gels and transferred onto nitrocellulose membranes. The membranes were then incubated with 7% skim milk at room temperature for 2 h, followed by incubation with primary and secondary antibodies at room temperature for 4 and 2 h, respectively. Finally, the membranes were imaged with an automated chemiluminescence system (Tanon-5200, China), and the results were quantified using ImageJ software.

2.14. Transcriptome Sequencing. After treating 143B cells with 0 or 100 μg/mL PMMENs for 24 h, total RNA was extracted using TransZol UP. Sequencing was performed using the Illumina platform, and data were analyzed using the bioinformatics analysis process provided by BMKCloud (www.biocloud.net), the cloud platform of Bemac.

2.15. LC-QTOF Platform-Based Metabolomic Analysis. Six PMMEN-treated groups and a control group were set up for metabolomics studies. Cells were treated with or without 100 μg/mL PMMENs for 24 h and collected in 1.5 mL EP tubes, which were snap-frozen in liquid nitrogen to quench the intracellular metabolites. Samples were transferred to EP tubes in three aliquots (300, 300, and 400 μL) with 1000 μL extract containing internal standard (1:1 v/v methanol−acetonitrile, internal standard concentration: 20 mg/L) and vortexed and mixed for 30 s. Steel beads were added to the samples and placed in a 45 Hz grinder for 10 min, sonicated for 10 min in an ice bath, and then rested at −20 °C for 1 h. The samples were centrifuged at 4 °C for 15 min at 12,000 rpm, and 500 μL of the supernatant was carefully removed from the EP tube. The extract was dried in a vacuum concentrator. Then, 160 μL of extract (1:1 v/v acetonitrile−water) was added to the dried metabolites, vortexed for 30 s, and sonicated for 10 min in an ice bath. The samples were then centrifuged at 4 °C for 15 min at 12,000 rpm, and 120 μL of the supernatant was carefully removed from the 2 mL injection vial. Next, 10 μL of the sample was mixed into QC samples for testing, and the injection volume was 1 μL. Metabolomic analysis was performed using an ultra-high-performance liquid chromatograph (Acquity I-Class PLUS) in tandem with a high-resolution mass spectrometer (Xevo G2-XS QTOF).

2.16. Quantitative Real-Time Polymerase Chain Reaction. Total RNA was extracted from the samples using the Trizol reagent following the manufacturer's instructions. The extracted RNA was quantified using NanoDrop2000 (ThermoFisher Scientific), and cDNA was synthesized using a reverse transcription kit. Subsequently, quantitative real-time polymerase chain reaction (qRT-PCR) was performed using ChamQ Universal SYBR qPCR Master Mix on the ABI StepOne Plus System (Life Technologies). β-actin was used as the internal reference for other RNAs. The PCR for each sample was repeated three times, and the $2^{-\Delta\Delta Ct}$ method was used to calculate relative expression values. The primer used in this experiment was provided by Sangon Biotech Co., Ltd. and is listed in Table S1.

2.17. Tumor Xenografts. Female BALA/c-nude mice (6−8 weeks old) (Weitong Lihua Laboratory Animal Technology Co., Ltd.) were used to investigate the anti-tumor activity of PMMENs against osteosarcoma. Briefly, 143B cells were digested, and the final concentration was adjusted to 1×10^7 cells/mL in PBS. A volume of 100 μL cell suspension was injected into the right subcutaneous flanks of mice. Once the subcutaneous tumor volume reached 50 mm^3, the mice were randomly divided into three groups: blank control (injected with 100 μL PBS), low dose group (1 mg/kg PMMENs in 100 μL PBS), and high dose group (10 mg/kg PMMENs in 100 μL PBS), with four mice in each group. The treatments were administered through the tail vein once every two days for a week. The long diameter (a) and short diameter (b) of tumors were measured using a vernier caliper every day during treatment, and the tumor volume (TV) was calculated using the following formula: $TV = a \times b^2 \times 1/2$. The mice were sacrificed after 24 h of the last administration. The tumors were removed and weighed. This study was approved by the Animal Ethics Committee of Guangdong Ocean University, Zhanjiang, China.

https://doi.org/10.1021/acsami.2c21485
ACS Appl. Mater. Interfaces 2023, 15, 26227−26240

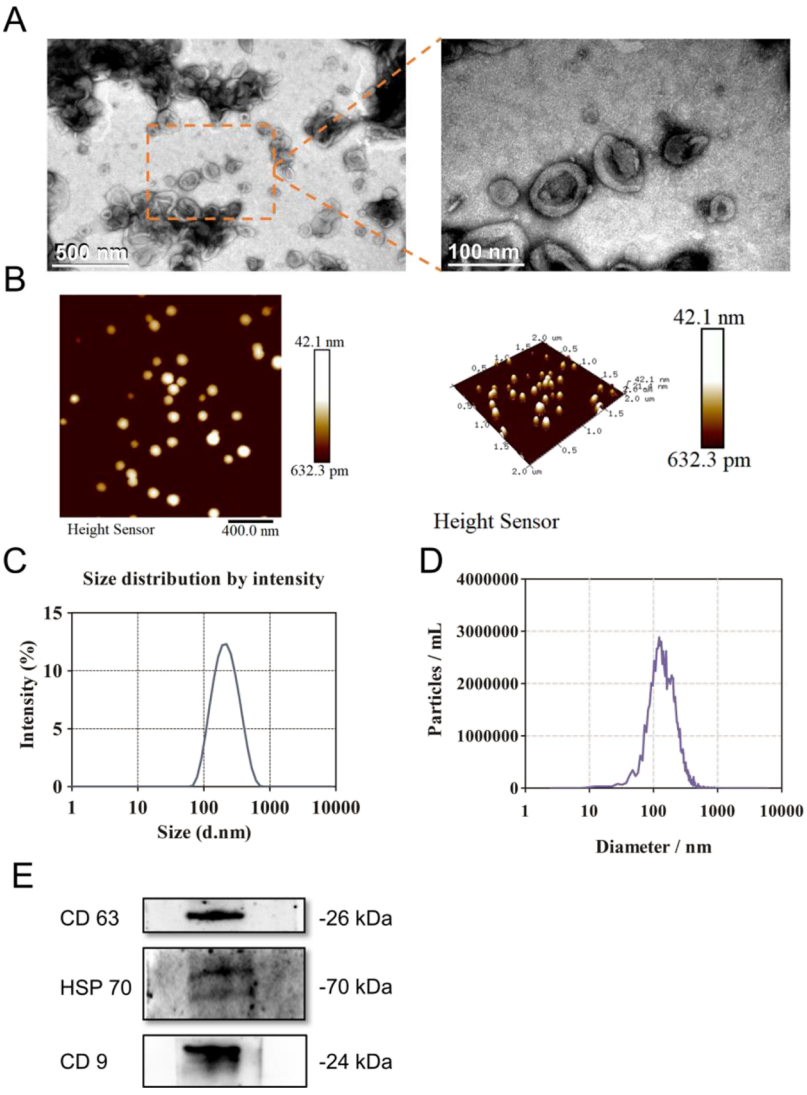

Figure 1. Characterization of PMMENs. (A) TEM images of PMMENs. Scale bars: 500 and 100 nm. (B) AFM images of PMMENs, including 2D and 3D morphology plots. (C) DLS analysis indicating the particle size distribution of PMMENs. (D) NTA indicating the particle size and concentration of PMMENs. (E) Western blot analysis of EV biomarkers, including CD63, HSP70, and CD9, in PMMENs.

2.18. Data Processing and Analysis. All data were analyzed using GraphPad Prism5 software. Results are expressed as mean ± standard deviation (S.D.). All experiments were performed independently three times. Statistical analysis between groups was performed using a *t*-test or one-way analysis of variance (ANOVA). $P < 0.05$ was considered statistically significant.

3. RESULTS AND ANALYSIS

3.1. PMMEN Isolation and Characterization. Exosome-like nanovesicles were extracted from *P. martensii* mucilage through differential centrifugation. TEM and AFM images showed that PMMENs had a cuplike morphology, and intact vesicles were isolated (Figure 1A,B). DLS results showed that the average hydrodynamic particle size of PMMENs was 193.3 nm, and the polydispersity index (PDI) was 0.186 (Figure 1C). In contrast, NTA results showed that the particle size and concentration of the PMMENs were 180.3 nm and 2.7×10^{12} particles/mL, respectively (Figure 1D). Protein immunoblotting confirmed the presence of CD63, HSP70, and CD9, the signature proteins of EVs, in PMMENs (Figure 1E). The above results demonstrate that the nanovesicles extracted from *P. martensii* mucilage are exosome-like nanoparticles.

3.2. PMMENs Inhibit 143B Cell Growth. PMMENs can function in 143B cells after successful uptake by the cells. To determine successful cellular uptake, PMMENs were labeled using PKH67 dye and co-incubated with the cells for 24 h. The results showed that green fluorescent PMMENs entered 143B cells (Figure 2A). In contrast, the blank control group showed no green fluorescence inside the cells, indicating successful uptake of PMMENs by the cells in the experimental group. Confocal imaging analysis further demonstrated that PMMENs were localized inside the cell membrane and internalized by the cells rather than being bound to the cell membrane surface.

Next, the effect of various PMMENs concentrations on 143B cell viability was investigated using the CCK-8 assay (Figure 2B). Low PMMENs concentrations (<10 μg/mL) had almost no effect on 143B cell viability; 143B cell viability significantly decreased ($P < 0.001$) after increasing PMMENs concentration to >50 μg/mL. To compare the effects of PMMENs on tumor and nontumor cells, as well as different tumor cell lines, four additional human cell lines were used: HepG-2, HUVEC, AGS, and hFOB 1.19 cells. PMMENs in the

https://doi.org/10.1021/acsami.2c21485
ACS Appl. Mater. Interfaces 2023, 15, 26227−26240

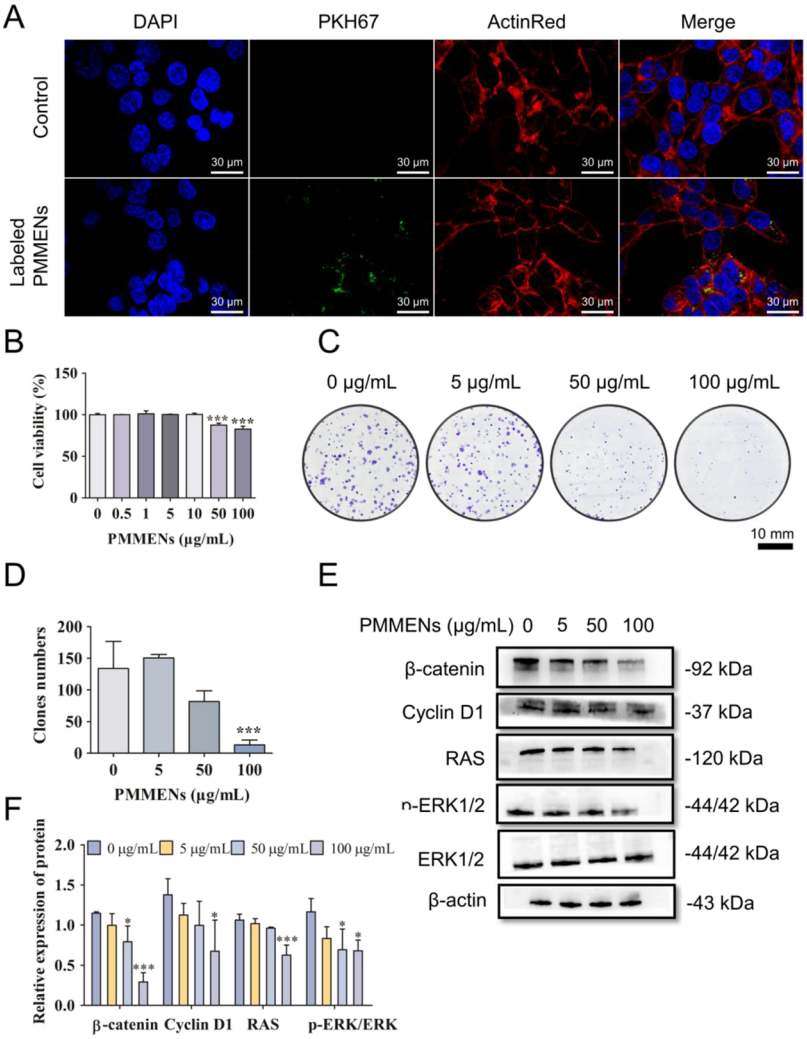

Figure 2. PMMENs inhibit 143B cell activity. (A) Confocal microscopy (40×) images of 143B cells with or without PKH67-labeled PMMENs. The nuclei, cytoskeleton, and PMMENs were stained with DAPI (blue), ActinRed (red), and PKH67 (green), respectively. (B) Cell Counting Kit-8 (CCK-8) assay to analyze 143B cell viability after co-incubation with different concentrations of PMMENs for 24 h. (C) Representative images of clone formation, and (D) quantification of 143B cells treated with different PMMENs concentrations. (E, F) Western blot analysis of β-catenin, cyclin D1, RAS, ERK1/2, and p-ERK protein expression in 143B cells. Significant differences are indicated by $^{*}P < 0.05$, $^{**}P < 0.01$, and $^{***}P < 0.001$.

range of 0−500 μg/mL did not affect the cell viability of HepG-2, HUVEC, and AGS cells (Figure S1A−C). In hFOB 1.19 cells, PMMENs had no significant cytotoxic effect on osteoblasts at 0−200 μg/mL levels. However, when the concentration of PMMENs reached 500 μg/mL, the cell viability of hFOB 1.19 cells was significantly inhibited (Figure S1D). PMMENs could significantly inhibit 143B cell viability at concentrations of 100, 150, and 200 μg/mL, but there was no significant difference in the inhibition effect at the concentration of 100−200 μg/mL. When the incubation concentration reached 500 μg/mL, the cell viability of 143B cells was reduced to less than 50% (Figure S1E). These results indicate that PMMENs have significant anti-tumor activity against 143B cells and are specific to 143B cells at concentrations less than 200 μg/mL. In the process of anti-tumor drug development, the ideal drug should only target tumor cells and have minimal toxic effects on healthy tissues. Therefore, we selected the concentration range of PMMENs that did not affect the viability of hFOB 1.19 cells, namely, 0, 5, 50, and 100 μg/mL, for further evaluation in other assays.

To assess the ability of PMMENs to inhibit 143B cell proliferation in vitro, clonogenic assays were performed with PMMEN-treated cells (Figure 2C,D). PMMENs (5 μg/mL) promoted 143B cell proliferation compared to the blank control; however, the difference was not statistically significant ($P > 0.05$); this may be because PMMENs inherently contain nutrients required by the cells, such as proteins and lipids.[16] In contrast, 50 and 100 μg/mL PMMENs significantly inhibited 143B cell clone formation in a dose-dependent manner. The development of human tumors involves six biological capabilities, including sustaining proliferative signaling, evading growth suppressors, resisting cell death, enabling replicative immortality, angiogenesis, and activating invasion and metastasis, and the inhibition of "proliferative signaling",[34] can be used as therapeutic targets to achieve the purpose of treatment. Restriction of tumor cell proliferation is an expected feature of compounds with anti-cancer potential.[35,36] To study the potential mechanism of PMMENs inhibiting cell proliferation, we analyzed the effect of PMMENs on cell proliferation-related signaling pathways using western blotting. Studies have shown

https://doi.org/10.1021/acsami.2c21485
ACS Appl. Mater. Interfaces 2023, 15, 26227−26240

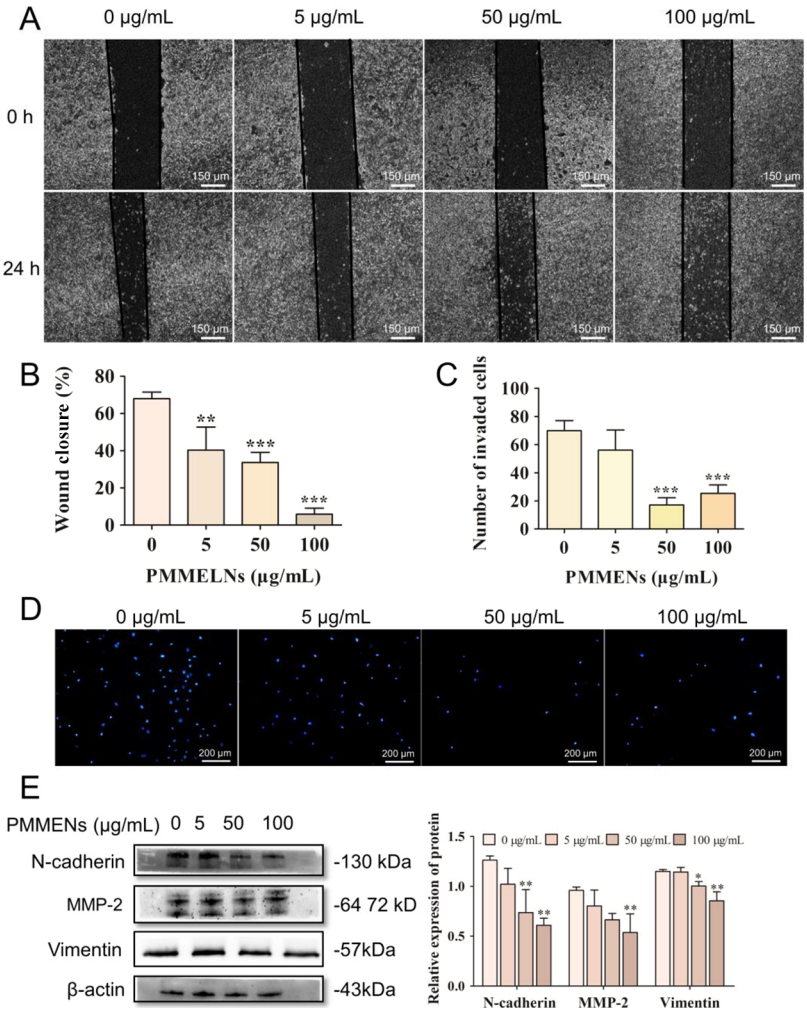

Figure 3. PMMENs inhibit 143B cell migration and invasion. (A) Representative images of wound healing assay of 143B cells treated with 0, 5, 50, and 100 μg/mL PMMENs for 24 h and (B) quantification. (C) Quantification and (D) representative images of invasion assays of 143B cells treated with 0, 5, 50, and 100 μg/mL PMMENs for 12 h. (E) Western blot images and quantification of N-cadherin, vimentin, and MMP-2 protein expression in 143B cells treated with different concentrations of PMMENs. Significant differences are indicated by $^{*}P < 0.05$, $^{**}P < 0.01$, and $^{***}P < 0.001$.

that the abnormality of the Wnt signaling pathway plays a key role in the occurrence and development of osteosarcoma.[37] The Wnt signaling pathway mainly consists of a series of protein kinases and transcription factors, which can regulate tumor growth, cell senescence, cell death, differentiation, and migration.[38] The expression of β-catenin is significantly upregulated in osteosarcoma cell lines compared with that in normal human osteoblasts, and downregulated β-catenin expression can significantly reduce the proliferation and colony formation of osteosarcoma cells. β-catenin has potential value as a prognostic marker of osteosarcoma.[35] Therefore, we propose that the Wnt signaling pathway may be involved in the inhibitory effect of PMMENs on the progression of osteosarcoma. The results showed that PMMENs inhibited the expression levels of β-catenin and its target protein cyclin D1 in a concentration-dependent manner, and the inhibition effect reached the maximum at 100 μg/mL PMMEN treatment (Figure 2E,F). Cyclin D1, a proto-oncogene associated with the infinite proliferation of tumor cells, is one of the proteins involved in cell mitosis.[39] While the effects of individual cyclins on normal tissue proliferation are largely dispensable, these proteins are essential for the proliferation of specific cancer types.[40,41] Cyclin D1 is highly expressed in a variety of cancers, including hepatocellular carcinoma,[42] melanoma,[43] myeloma,[39] and ovarian cancer.[44] The anti-tumor activity of many naturally extracted compounds is also related to the regulation of cyclin D1, for example, quercetin[45] and casearin D[46] extracted from plants, whose biological activity is related to the inhibition of cyclin D1 expression. The RAS−RAF−MEK−ERK (ERK1/2) signaling pathway plays an important role in transmitting extracellular signals to cells. In the ERK1/2 signal pathway, ERK1/2, as an effector kinase of the upstream signal, plays a key role in signal transduction. ERK1/2 is involved in the regulation of various tumor-related biological processes, including cell proliferation, differentiation, and migration, by inhibiting or enhancing the activity of target proteins through phosphorylation.[47] The ERK1/2 signaling pathway has been extensively researched and reviewed to identify new target-based cancer therapies,[48] and many inhibitors of Ras and ERK have been developed to target different targets in the ERK1/2 signal. Some of these drugs have been approved for use. In the present study, PMMEN treatment downregulated the expression of RAS, p-ERK, and cyclin D1 in 143B cells (Figure 2E,F). Our results suggest that PMMENs may effectively

https://doi.org/10.1021/acsami.2c21485
ACS Appl. Mater. Interfaces 2023, 15, 26227−26240

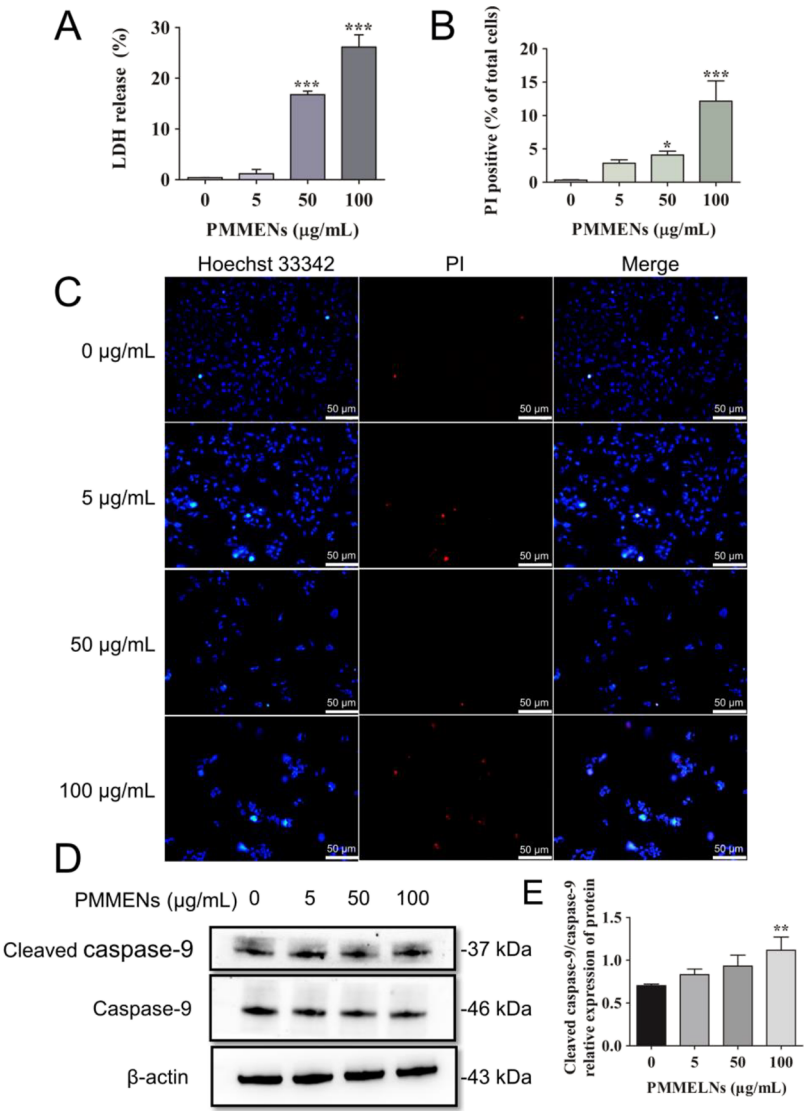

Figure 4. PMMENs induce apoptosis. (A) Effect of PMMENs on LDH release from 143B cells was determined using the LDH release assay. (B) Quantification of the percentage of PI-positive cells. (C) Representative images of Hoechst 33342 (blue) and PI (red) double fluorescence staining of 143B cells after treatment with different concentrations of PMMENs for 24 h. Quantification of the percentage of PI-positive cells. Scale bar: 50 μm. (D, E) Western blot analysis of cleaved caspase-9 and caspase-9 protein expression levels in 143B cells. Significant differences are indicated by $^{*}P < 0.05$, $^{**}P < 0.01$, and $^{***}P < 0.001$.

induce the downregulation of cyclin D1 through Wnt and ERK1/2 signaling pathways, thereby inhibiting the proliferation of 143B cells.

3.3. PMMENs Inhibit 143B Cell Migration and Invasion. Tumor metastasis is a complex process in the development of cancer, involving tumor cell detachment, extracellular matrix degradation, infiltration, and epithelial-mesenchymal transition (EMT). EMT is closely associated with the invasiveness and migratory capacity of tumor cells, where mesenchymal markers include N-cadherin and vimentin. Matrix metalloproteinases, such as MMP-2, are significantly upregulated in osteosarcoma and metastasis and indicate poor prognosis.[49] Studies have shown that MMP-2 downregulation inhibits osteosarcoma metastasis and infiltration.[50] To investigate whether PMMENs can inhibit 143B cell invasion and migration, the cells were treated with different concentrations of PMMENs for 24 h. The results of wound healing experiments showed that 5, 50, and 100 μg/mL PMMENs significantly inhibited cell migration in a dose-dependent manner compared to blank controls (Figure 3A,B). Invasion assay results showed that the number of invading 143B cells significantly decreased after treatment with 50 and 100 μg/mL PMMENs ($P < 0.001$; Figure 3C,D). Furthermore, protein immunoblotting results showed that N-cadherin, vimentin, and MMP-2 protein expression levels decreased in a dose-dependent manner after PMMEN treatment (Figure 3E). Taken together, these results suggest that PMMENs inhibit 143B osteosarcoma cell invasion and migration by suppressing EMT and downregulating MMP-2.

3.4. PMMENs Induce Apoptosis in 143B Cells. Apoptosis plays a crucial role in maintaining a homeostatic balance between cell survival and mortality in several biological processes. Disrupting this balance may lead to abnormal cell growth, proliferation, or autoimmune diseases.[51] LDH, a stable cytoplasmic enzyme, is present in all cells and released in the cell culture medium after rupturing cell membrane structures due to apoptosis or necrosis, which is a key feature of cells undergoing apoptosis, necrosis, and other forms of cell

https://doi.org/10.1021/acsami.2c21485
ACS Appl. Mater. Interfaces 2023, 15, 26227−26240

damage.[52] We examined the rate of LDH release from 143B cells after co-incubating them with PMMENs for 24 h using an LDH kit. Compared to the blank control, 50 and 100 μg/mL PMMENs significantly increased the rate of LDH release from 143B cells (Figure 4A). Therefore, PMMENs may induce apoptosis in 143B cells. To further confirm these results, 143B cells were stained with Hoechst 33342 and PI. The percentage of live cells decreased, and the percentage of PI-positive cells gradually increased with increasing PMMEN concentrations, indicating that PMMENs induced cell death in a dose-dependent manner (Figure 4B,C). Additionally, protein immunoblotting results showed that the ratio of cleaved caspase-9 to caspase-9 expression levels gradually increased compared with that in the blank control group, which was positively correlated with the PMMEN concentration (Figure 4D,E). These data suggest that PMMENs induce apoptosis in 143B cells.

3.5. Transcriptomic Analysis of PMMEN-Treated 143B Cells. Based on the above results, 100 μg/mL PMMENs had a more significant effect on 143B cells than 0, 5, or 50 μg/mL PMMENs. Therefore, to evaluate the effect of PMMENs on gene expression in 143B cells, transcriptome sequencing and bioinformatics analysis were performed on 143B cells treated with 100 μg/mL PMMENs (PMMENs group) and 0 μg/mL PMMENs (control group). To detect differentially expressed genes (DEGs), fold change ≥1.5 and FDR < 0.05 were used as screening criteria. In total, 587 DEGs were identified between cells in the control and PMMENs groups, of which 392 genes were upregulated, and 195 genes were downregulated (Figure 5A).

The functions of the DEGs were further elucidated using Gene Ontology (GO) and Kyoto Encyclopedia of Genes and Genomes (KEGG) pathway enrichment analysis. GO enrichment analysis revealed that PMMENs contained DEGs highly enriched in biological processes regulating programmed cell death and cell death (Figure 5B). To further understand the enriched pathways of these DEGs between the control and PMMENs groups, KEGG pathway analysis was performed, which revealed that the DEGs were closely associated with cancer signaling pathways (Figure 5C).

3.6. Metabolomic Analysis of PMMEN-Treated 143B Cells. To investigate the changes in the metabolic profile of 143B cells after PMMEN treatment, LC-QTOF was used to detect positive and negative ion modes of the control and PMMENs groups, and the obtained raw data were analyzed using Progenesis QI software. A supervised orthogonal projection to latent structures discriminant analysis (OPLS-DA) model was constructed to evaluate the differences between the control and PMMEN groups (Figure 6). The R2Y and Q2Y values were 0.992 and 0.955 for the positive (Figure 6A) and 0.988 and 0.961 for the negative (Figure 6B) ion OPLS-DA models, respectively, indicating the stability and reliability of the model. The intracellular metabolites were significantly different between the control and PMMENs groups, indicating that PMMENs significantly changed the metabolic profile of 143B cells. Using $P < 0.05$ in one-way statistics or VIP > 1 in multi-factor statistics, 661 and 568 differentially accumulated metabolites (DAMs) were identified in the positive and negative ion models, respectively.

The DAMs were mainly enriched in arachidonic acid metabolism, D-amino acid metabolism, and 12-, 14-, and 16-membered macrolide biosynthetic pathways (Figure 6C). In addition, they were involved in pantothenic acid and coenzyme

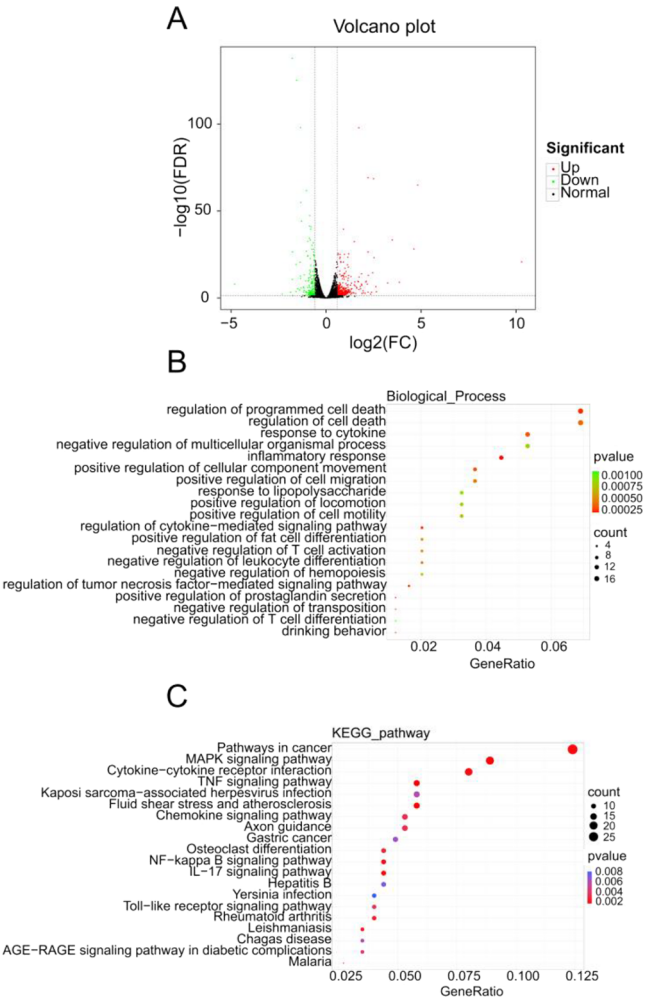

Figure 5. Changes in gene expression in PMMENs-treated 143B cells. (A) Volcano plot of DEGs. Red and green represent upregulated and downregulated DEGs, respectively. (B) GO enrichment bubble plot and (C) KEGG-enriched pathways of DEGs.

A synthesis, cyclic adenosine monophosphate (cAMP) signaling pathway, arginine biosynthesis, cysteine and methionine metabolism, lysine degradation, and other amino acid synthetic and metabolic processes. Figure 6D shows the changes of various metabolites in these signaling pathways. Amino acid metabolism affects the survival of various cancer cell lines and acts within the tumor and tumor microenvironment. For example, L-leucine and L-glutamine inhibit HepG-2 cell proliferation during their synthesis and metabolism, whereas L-methionine only affects HepG-2 cell viability.[53] Leucine deprivation also causes apoptosis in melanoma cells.[54] Inhibiting amino acid metabolism is an active area of cancer metabolism research,[55] and tyrosine kinase inhibitors, such as sorafenib and regorafenib, have been approved for treating advanced hepatocellular carcinoma in different regions of the world.[56]

3.7. Integrated Transcript and Metabolite Plots. The results of DAM and DEG analyses from transcriptomics were combined, and the DEGs and DAMs of the same groups were mapped to KEGG pathways for analysis (Figure S2). After treatment with PMMENs, DEGs and DAMs were mapped to 101 KEGG signaling pathways. Among them, cancer signaling pathways, such as the cAMP, Wnt, and MAPK signaling

https://doi.org/10.1021/acsami.2c21485
ACS Appl. Mater. Interfaces 2023, 15, 26227−26240

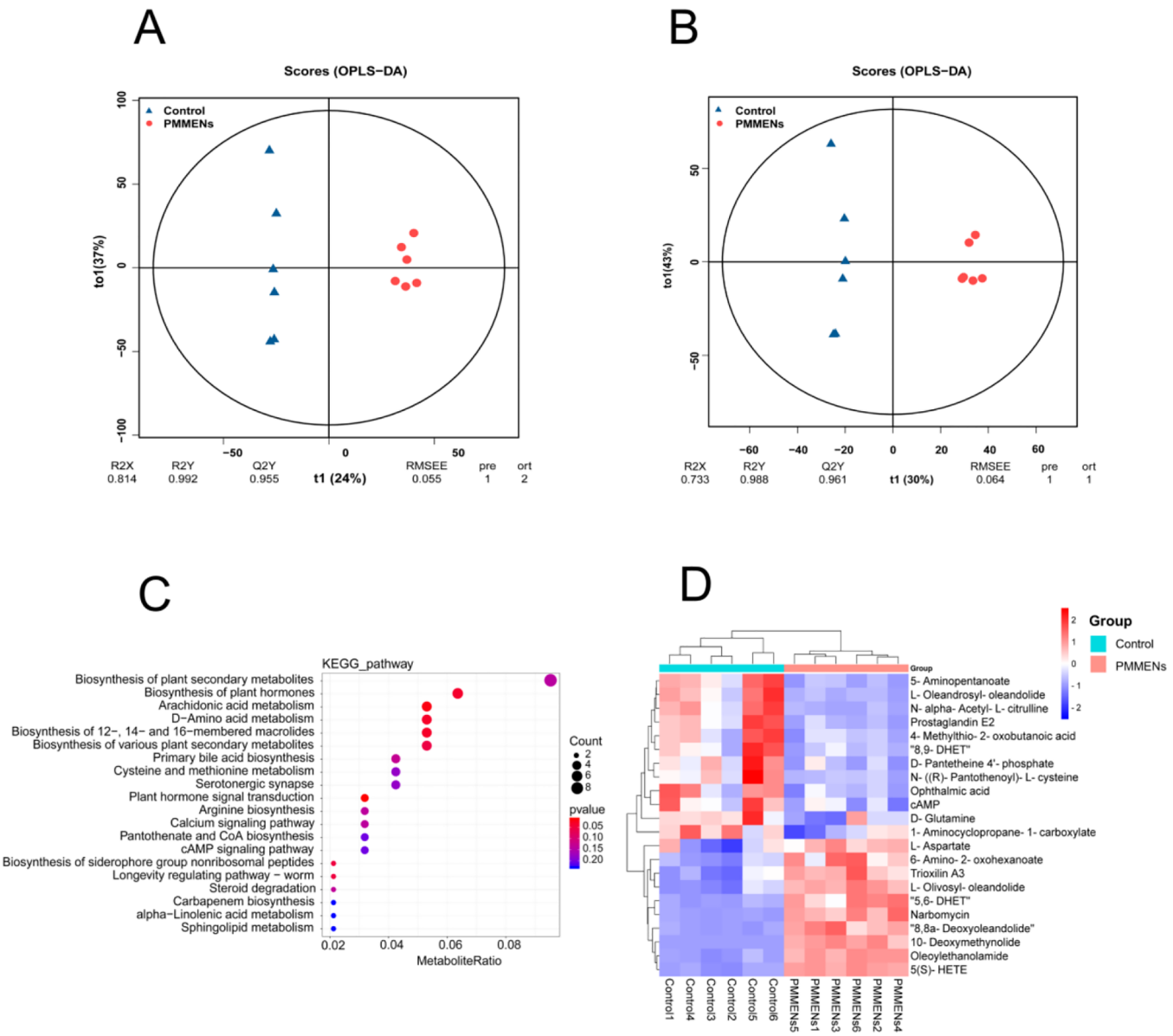

Figure 6. Changes in metabolite expression in PMMEN-treated 143B cells. Orthogonal projection to latent structures discriminant analysis (OPLS-DA) score plot of metabolite ions obtained in (A) positive and (B) negative ion modes. (C) KEGG enrichment bubble plots of DAMs and (D) heatmap showing upregulated and downregulated metabolites.

pathways, to which the DEGs and DAMs were jointly mapped for analysis, were selected. In the cancer signaling pathways, 28 DEGs and 2 DAMs were enriched, of which 12 DEGs were downregulated and 16 were upregulated (Figure 7A), and the DAMs of Prostaglandin E2 (PGE2) and cyclic adenosine monophosphate (cAMP) were downregulated.

Figure 7B shows the correlation between metabolites and genes in cancer signaling pathways. PGE2 was positively correlated with the expression of ENSG00000100311 (PDGFB), ENSG00000113721 (PDGFRB), and ENSG00000121966 (CXCR4) and negatively correlated with the expression of ENSG00000023445 (BIRC3), ENSG00000056558 (TRAF1), ENSG00000073756 (RTGS2), ENSG00000100906 (NFKBIA), ENSG00000102678 (FGF9), ENSG00000196611 (MMP1), Homo_sapiens_newGene_1764, and Homo_sapiens_newGene_2000.

Furthermore, cAMP was the first secondary messenger to be identified and plays a vital role in cell signaling and regulating many physiological and pathological processes.[57] cAMP directly regulates various biological processes and cellular behaviors, including metabolism, ion channel activation, gene expression, cell growth, differentiation, and apoptosis.[58] cAMP production is regulated by G protein-dependent or -independent mechanisms. Upon extracellular ligand PGE2 binding to G protein-coupled receptors (GPCRs), the Gα subunit separates from the Gβ and Gγ subunits and activates adenylate cyclases (ACs), converting ATP to cAMP.[59] cAMP signaling has both tumor-suppressive and oncogenic effects, depending on the cell type and the environment in which it is located. For example, PKA activation by increasing cAMP levels or providing cAMP analogs (dcAMP and 8-BrcAMP) decreases the proliferation rate, promotes differentiation, and induces apoptosis of A-172 cells in brain tumors.[60] In contrast, vasoactive intestinal peptide reduces cAMP concentration, CREB expression, and

https://doi.org/10.1021/acsami.2c21485
ACS Appl. Mater. Interfaces 2023, 15, 26227−26240

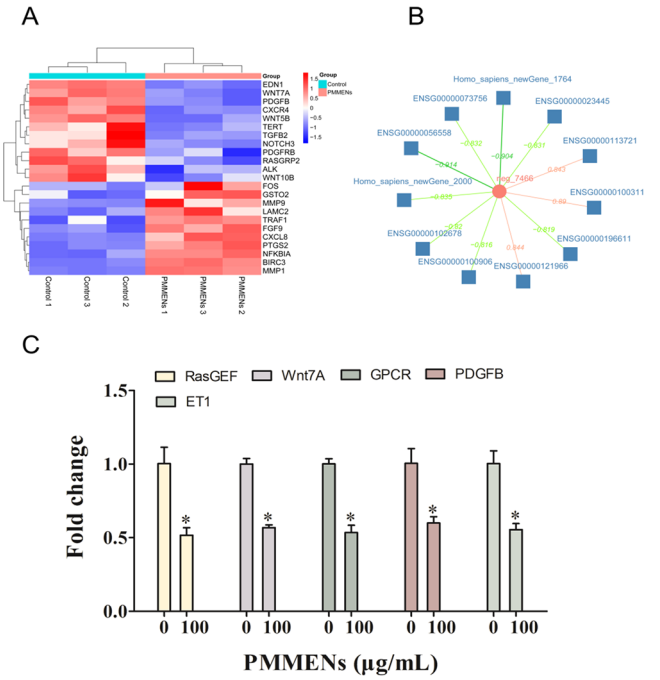

Figure 7. Joint transcriptome and metabolome enrichment analysis. (A) Heat map of DEGs in cancer signaling pathways. (B) Correlation network diagram of DAMs and DEGs in cancer signaling pathways. (C) Expression levels of RasGEF, Wnt7A, GPCR, PDGFB, and ET1 were detected using RT-qPCR.

Ser133 phosphorylation; inhibits Bcl-xl expression; and induces apoptosis in Huh7 cells.[61] Decreased cAMP levels may inhibit cell growth, and PDE4-activating compounds reduce intracellular cAMP levels, thereby inhibiting renal cyst formation.[62] PKA is one of the primary targets of cAMP, and PKA antagonists inhibit β-catenin and c-myc nuclear translocation and COX2 expression in colorectal cancers with APC mutations, thereby inhibiting cancer development and progression.[62] Endothelin 1 (ET1) is involved in several cancer-related processes, including cell proliferation, apoptosis, matrix remodeling, and metastasis. ET1 significantly induces MMP2 synthesis and activity dose-dependently to induce OS cell migration and survival.[63,64] Transcriptomic and metabolomic analyses showed that GPCR, ET1, PGE2, and cAMP were downregulated after PMMEN treatment, which may be related to the ability of PMMENs to inhibit 143B cell proliferation.

Protein immunoblotting results suggest that the mechanism of PMMEN-mediated cell proliferation inhibition may involve the ERK1/2 and Wnt signaling pathways. The ERK1/2 signaling pathway plays an essential role in regulating cell proliferation, differentiation, apoptosis, and migration and can be activated by different extracellular stimuli, such as cytokines, neurotransmitters, and hormones. Platelet-derived growth factor subunit B (PDGF-B) is a growth factor in the PDGF family that plays a crucial role in embryonic development and adult wound healing by binding and activating the corresponding platelet-derived growth factor receptors (PDGFRs).[65] PDGFRs are catalytic receptors with intracellular tyrosine

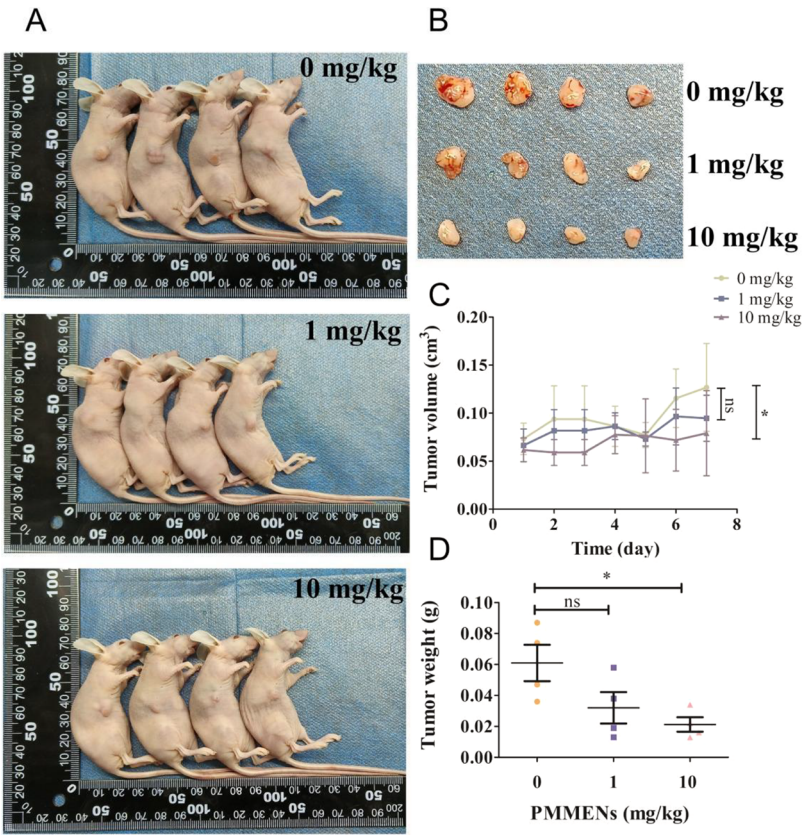

Figure 8. PMMENs suppress osteosarcoma growth in vivo. (A) Growth curve of xenografts in nude mice. (B) Samples of the tumor after treatment. (C) Changes in tumor volume in vivo after treatment. (D) Weight of tumors. Significant differences are indicated by $^{*}P < 0.05$, $^{**}P < 0.01$, and $^{***}P < 0.001$.

https://doi.org/10.1021/acsami.2c21485
ACS Appl. Mater. Interfaces 2023, 15, 26227−26240

kinase activity. As targeted receptors for extracellular stimulation, PDGFRs regulate many biological processes, including proliferation, differentiation, angiogenesis, and tumor metastasis.[66−68] PDGFR inhibition also enhances the pro-apoptotic effects of the associated apoptosis-inducing ligand TRAIL.[69] Ras guanine nucleotide exchange factor 2 (RasGEF) is an important protein that acts as a molecular switch for intracellular signaling to activate RAS.[15] Anaplastic lymphoma kinase (EML4-ALK) is a receptor tyrosine kinase that induces ERK1/2 phosphorylation.[70] Our results show that PMMEN treatment downregulated PDGF, PDGFR, RasGEF, and EML4AIK gene expression, which may inhibit RAS expression and ERK phosphorylation. Consistent with the results of protein immunoblotting, PMMENs may promote ERK1/2 signaling pathway inactivation, thereby inhibiting cell proliferation. ERK1/2 signaling pathway inactivation also inhibits tumor cell migration and invasion.[71] Our findings suggest that PMMENs may be involved in regulating cell migration and invasive ability through the ERK1/2 signaling pathway. Activated ERK regulates several cellular activities, including cell proliferation and migration. Recently, compounds targeting ERK signaling pathway components, such as RAF or MEK inhibitors, have significantly improved clinical outcomes in metastatic melanoma and have shown promising clinical activity in other tumor types.[72−74] Developing RAS and ERK inhibitors shows great potential in the fight against cancer.

The Wnt signaling pathway plays a crucial role in cancer progression by acting as an autocrine and paracrine signaling molecule between Wnt-producing and -receiving cells.[75] The involvement of the Wnt pathway in the anti-tumor effects of drugs has been investigated by inhibiting Wnt activation using Wnt antagonists, such as RNF43 and ZNRF3.[76] Transcriptomic results showed that Wnt gene expression was reduced in the PMMENs group. Additionally, protein immunoblotting results demonstrated reduced β-catenin and cyclin D1 protein expression levels downstream of the Wnt signaling pathway, suggesting that PMMENs may prevent 143B cell proliferation by inhibiting the Wnt signaling pathway.

According to the combined analysis of transcriptomes and metabolomics, five genes, RasGEF, Wnt7A, GPCR, PDGFB, and ET1, were selected for the RT-qPCR experiment. The results are shown in Figure 7C. Compared with that in the control group, 100 μg/mL PMMEN treatment significantly downregulated the expression of RasGEF, Wnt7A, GPCR, PDGFB, and ET1, which was consistent with the results in Figure 7A. These findings indicate that the results of our omics data analysis were credible.

3.8. PMMENs Suppress Osteosarcoma Growth. A xenograft model of osteosarcoma was established using BALA/c-nude mice. In vivo experiments demonstrated that PMMENs significantly reduced the growth of tumor volume and tumor weight of osteosarcoma compared with that in the control group, and the inhibitory effect was more pronounced in the high-concentration group than in the low-concentration group (Figure 8A−D).

4. CONCLUSIONS

In conclusion, we isolated intact PMMENs with a cuplike morphology from *P. martensii* mucilage by ultracentrifugation. The PMMENs were found to be 180.3−193.3 nm in size and were taken up by 143B cells. PMMENs were shown to have anti-tumor activity as they dose-dependently inhibited 143B cell proliferation, migration, and invasion and induced apoptosis through mechanisms related to cancer signaling pathways. In summary, PMMENs with bioactive properties were isolated from pearl oyster *P. martensii* mucilage, which can inhibit the activation of the ERK1/2 and Wnt signaling pathways and the growth of osteosarcoma in mice. PMMENs have the potential to be ideal candidates in the development of novel drugs for cancer treatment.

■ ASSOCIATED CONTENT

Supporting Information

The Supporting Information is available free of charge at https://pubs.acs.org/doi/10.1021/acsami.2c21485.

Figures of cell viability of PMMENs on different cell lines and the co-enrichment pathway of DAMs and DEGs; and table of primers for real-time PCR (PDF)

■ AUTHOR INFORMATION

Corresponding Authors

Chengyong Li − *Shenzhen Institute of Guangdong Ocean University, Shenzhen 518108, P. R. China;* orcid.org/0000-0003-0018-165X; Email: cyli@gdou.edu.cn

Hao Lin − *Stem Cell Research and Cellular Therapy Center, Orthopedic Center, Affiliated Hospital of Guangdong Medical University, Zhanjiang 524001, P. R. China*; Email: linhao@gdmu.edu.cn

Authors

Peng Li − *Stem Cell Research and Cellular Therapy Center, Orthopedic Center, Affiliated Hospital of Guangdong Medical University, Zhanjiang 524001, P. R. China*

Lihua Ma − *Shenzhen Institute of Guangdong Ocean University, Shenzhen 518108, P. R. China; College of Food Science and Technology, Guangdong Ocean University, Zhangjiang 518108, P. R. China*

Weiqiang Zhan − *Stem Cell Research and Cellular Therapy Center, Orthopedic Center, Affiliated Hospital of Guangdong Medical University, Zhanjiang 524001, P. R. China*

Dong Xie − *Stem Cell Research and Cellular Therapy Center, Orthopedic Center, Affiliated Hospital of Guangdong Medical University, Zhanjiang 524001, P. R. China*

Guanhao Hong − *Stem Cell Research and Cellular Therapy Center, Orthopedic Center, Affiliated Hospital of Guangdong Medical University, Zhanjiang 524001, P. R. China*

Mingzhu Deng − *Stem Cell Research and Cellular Therapy Center, Orthopedic Center, Affiliated Hospital of Guangdong Medical University, Zhanjiang 524001, P. R. China*

Zijie Wu − *Shenzhen Institute of Guangdong Ocean University, Shenzhen 518108, P. R. China; College of Food Science and Technology, Guangdong Ocean University, Zhangjiang 518108, P. R. China*

Peichun Lin − *Shenzhen Institute of Guangdong Ocean University, Shenzhen 518108, P. R. China*

Linhong Yan − *Shenzhen Institute of Guangdong Ocean University, Shenzhen 518108, P. R. China; College of Food Science and Technology, Guangdong Ocean University, Zhangjiang 518108, P. R. China*

Zifan Lu − *Shenzhen Institute of Guangdong Ocean University, Shenzhen 518108, P. R. China*

Complete contact information is available at: https://pubs.acs.org/10.1021/acsami.2c21485

Author Contributions

P.L. and L.M. have contributed equally to this work and share first authorship. P.L. and L.M.: Investigation, data curation, formal analysis, writing − original draft. W.Z., D.X., and P.L.: Investigation. M.D., G.H., and L.Y.: Visualization. Z.W.: methodology, writing-review, and editing. Z.L.: Writing-review and editing. C.L. and H.L.: Writing-review and editing, funding acquisition.

Notes

The authors declare no competing financial interest.

■ ACKNOWLEDGMENTS

This work was supported by the National Natural Science Foundation of China (81570260), Science and Technology Program of Zhanjiang, China (2021A05069), Special Funds for Science Technology Innovation and Industrial Development of Shenzhen Dapeng New District (KJYF202001-06), Doctor Foundation of the Affiliated Hospital of Guangdong Medical University (BJ201802), Special fund for Affiliated Hospital of Guangdong Medical University "Clinical Medicine +" CnTech Co-construction Platform (CLP2021A001), and Open funding of Affiliated Hospital of Guangdong Medical University-research of autophagy and diseases.

■ REFERENCES

(1) Belayneh, R.; Fourman, M. S.; Bhogal, S.; Weiss, K. R. Update on Osteosarcoma. *Curr. Oncol. Rep.* **2021**, *23*, 71.
(2) Simpson, E.; Brown, H. L. Understanding osteosarcomas. *JAAPA* **2018**, *31*, 15−19.
(3) Marko, T. A.; Diessner, B. J.; Spector, L. G. Prevalence of Metastasis at Diagnosis of Osteosarcoma: An International Comparison. *Pediatr. Blood Cancer* **2016**, *63*, 1006−1011.
(4) Harris, M. A.; Hawkins, C. J. Recent and Ongoing Research into Metastatic Osteosarcoma Treatments. *Int. J. Mol. Sci.* **2022**, *23*, 3817.
(5) Huang, X.; Zhao, J.; Bai, J.; Shen, H.; Zhang, B.; Deng, L.; Sun, C.; Liu, Y.; Zhang, J.; Zheng, J. Risk and clinicopathological features of osteosarcoma metastasis to the lung: A population-based study. *J. Bone Oncol.* **2019**, *16*, No. 100230.
(6) Carrle, D.; Bielack, S. S. Current strategies of chemotherapy in osteosarcoma. *Int. Orthop.* **2006**, *30*, 445−451.
(7) Ferrari, S.; Briccoli, A.; Mercuri, M.; Bertoni, F.; Picci, P.; Tienghi, A.; Del Prever, A. B.; Fagioli, F.; Comandone, A.; Bacci, G. Postrelapse survival in osteosarcoma of the extremities: prognostic factors for long-term survival. *J. Clin. Oncol.* **2003**, *21*, 710−715.
(8) Anninga, J. K.; Gelderblom, H.; Fiocco, M.; Kroep, J. R.; Taminiau, A. H.; Hogendoorn, P. C.; Egeler, R. M. Chemotherapeutic adjuvant treatment for osteosarcoma: where do we stand? *Eur. J. Cancer* **2011**, *47*, 2431−2445.
(9) Ferrari, S.; Serra, M. An update on chemotherapy for osteosarcoma. *Expert Opin. Pharmacother.* **2015**, *16*, 2727−2736.
(10) Doyle, L. M.; Wang, M. Z. Overview of Extracellular Vesicles, Their Origin, Composition, Purpose, and Methods for Exosome Isolation and Analysis. *Cell* **2019**, *8*, No. 727.
(11) van Niel, G.; D'Angelo, G.; Raposo, G. Shedding light on the cell biology of extracellular vesicles. *Nat. Rev. Mol. Cell Biol.* **2018**, *19*, 213−228.
(12) Xu, K.; Liu, Q.; Wu, K.; Liu, L.; Zhao, M.; Yang, H.; Wang, X.; Wang, W. Extracellular vesicles as potential biomarkers and therapeutic approaches in autoimmune diseases. *J. Transl. Med.* **2020**, *18*, 432.
(13) He, C.; Zheng, S.; Luo, Y.; Wang, B. Exosome Theranostics: Biology and Translational Medicine. *Theranostics* **2018**, *8*, 237−255.
(14) Dai, J.; Su, Y.; Zhong, S.; Cong, L.; Liu, B.; Yang, J.; Tao, Y.; He, Z.; Chen, C.; Jiang, Y. Exosomes: key players in cancer and potential therapeutic strategy. *Signal Transduction Targeted Ther.* **2020**, *5*, 145.
(15) Takino, J. I.; Miyazaki, S.; Nagamine, K.; Hori, T. The Role of RASGRP2 in Vascular Endothelial Cells-A Mini Review. *Int. J. Mol. Sci.* **2021**, *22*, 11129.
(16) Chen, Q.; Li, Q.; Liang, Y.; Zu, M.; Chen, N.; Canup, B. S. B.; Luo, L.; Wang, C.; Zeng, L.; Xiao, B. Natural exosome-like nanovesicles from edible tea flowers suppress metastatic breast cancer via ROS generation and microbiota modulation. *Acta Pharm. Sin. B* **2022**, *12*, 907−923.
(17) Deng, Z.; Rong, Y.; Teng, Y.; Mu, J.; Zhuang, X.; Tseng, M.; Samykutty, A.; Zhang, L.; Yan, J.; Miller, D.; Suttles, J.; Zhang, H. G. Broccoli-Derived Nanoparticle Inhibits Mouse Colitis by Activating Dendritic Cell AMP-Activated Protein Kinase. *Mol. Ther.* **2017**, *25*, 1641−1654.
(18) Gratpain, V.; Mwema, A.; Labrak, Y.; Muccioli, G. G.; van Pesch, V.; des Rieux, A. Extracellular vesicles for the treatment of central nervous system diseases. *Adv. Drug Deliv. Rev.* **2021**, *174*, 535−552.
(19) Sahoo, S.; Losordo, D. W. Exosomes and cardiac repair after myocardial infarction. *Circ. Res.* **2014**, *114*, 333−344.
(20) Chen, J.; Chopp, M. Exosome Therapy for Stroke. *Stroke* **2018**, *49*, 1083−1090.
(21) Wang, B.; Guo, X.-J.; Cai, H.; Zhu, Y.-H.; Huang, L.-Y.; Wang, W.; Luo, L.; Qi, S.-H. Momordica charantia-derived extracellular vesicles-like nanovesicles inhibited glioma proliferation, migration, and invasion by regulating the PI3K/AKT signaling pathway. *J. Funct. Foods* **2022**, *90*, No. 104968.
(22) Cui, W. W.; Ye, C.; Wang, K. X.; Yang, X.; Zhu, P. Y.; Hu, K.; Lan, T.; Huang, L. Y.; Wang, W.; Gu, B.; Yan, C.; Ma, P.; Qi, S. H.; Luo, L. Momordica. charantia-Derived Extracellular Vesicles-Like Nanovesicles Protect Cardiomyocytes Against Radiation Injury via Attenuating DNA Damage and Mitochondria Dysfunction. *Front. Cardiovasc. Med.* **2022**, *9*, No. 864188.
(23) Yang, M.; Liu, X.; Luo, Q.; Xu, L.; Chen, F. An efficient method to isolate lemon derived extracellular vesicles for gastric cancer therapy. *J. Nanobiotechnol.* **2020**, *18*, 100.
(24) Oeyen, E.; Van Mol, K.; Baggerman, G.; Willems, H.; Boonen, K.; Rolfo, C.; Pauwels, P.; Jacobs, A.; Schildermans, K.; Cho, W. C.; Mertens, I. Ultrafiltration and size exclusion chromatography combined with asymmetrical-flow field-flow fractionation for the isolation and characterisation of extracellular vesicles from urine. *J. Extracell. Vesicles* **2018**, *7*, No. 1490143.
(25) De Robertis, M.; Sarra, A.; D'Oria, V.; Mura, F.; Bordi, F.; Postorino, P.; Fratantonio, D. Blueberry-Derived Exosome-Like Nanoparticles Counter the Response to TNF-alpha-Induced Change on Gene Expression in EA.hy926 Cells. *Biomolecules* **2020**, *10*, 742.
(26) Ju, S.; Mu, J.; Dokland, T.; Zhuang, X.; Wang, Q.; Jiang, H.; Xiang, X.; Deng, Z. B.; Wang, B.; Zhang, L.; Roth, M.; Welti, R.; Mobley, J.; Jun, Y.; Miller, D.; Zhang, H. G. Grape exosome-like nanoparticles induce intestinal stem cells and protect mice from DSS-induced colitis. *Mol. Ther.* **2013**, *21*, 1345−1357.
(27) Stanly, C.; Alfieri, M.; Ambrosone, A.; Leone, A.; Fiume, I.; Pocsfalvi, G. Grapefruit-Derived Micro and Nanovesicles Show Distinct Metabolome Profiles and Anticancer Activities in the A375 Human Melanoma Cell Line. *Cell* **2020**, *9*, 2722.
(28) Jo, S. H.; Kim, C.; Park, S. H. Novel Marine Organism-Derived Extracellular Vesicles for Control of Anti-Inflammation. *Tissue Eng. Regen. Med.* **2021**, *18*, 71−79.
(29) Liu, X.; Huang, L.; Bai, Y.; Liu, X.; Li, S. Extracting bio-zinc and taurine from Pinctada martensii meat. *J. Food Sci.* **2020**, *85*, 1125−1131.
(30) Yang, F.; Qin, X.; Zhang, T.; Zhang, C.; Lin, H. Effect of Oral Administration of Active Peptides of Pinctada Martensii on the Repair of Skin Wounds. *Mar. Drugs* **2019**, *17*, 697.
(31) He, J.; Shen, C.; Liang, H.; Fang, X.; Lu, J. Antimicrobial properties and immune-related gene expression of a C-type lectin isolated from Pinctada fucata martensii. *Fish Shellfish Immunol.* **2020**, *105*, 330−340.
(32) Magnadóttir, B.; Kraev, I.; Gudmundsdóttir, S.; Dodds, A. W.; Lange, S. Extracellular vesicles from cod (Gadus morhua L.) mucus

contain innate immune factors and deiminated protein cargo. *Dev. Comp. Immunol.* **2019**, *99*, No. 103397.
(33) Zhao, N.; Zhang, B.; Xu, Z.; Jia, L.; Li, M.; He, X.; Bao, B. Detecting Cynoglossus semilaevis infected with Vibrio harveyi using micro RNAs from mucous exosomes. *Mol. Immunol.* **2020**, *128*, 268−276.
(34) Hanahan, D.; Weinberg, R. A. Hallmarks of Cancer: The Next Generation. *Cell* **2011**, *144*, 646−674.
(35) Liu, W.; Zhao, Z.; Wang, Y.; Li, W.; Su, Q.; Jia, Q.; Zhang, J.; Zhang, X.; Shen, J.; Yin, J. Dioscin inhibits stem-cell-like properties and tumor growth of osteosarcoma through Akt/GSK3/β-catenin signaling pathway. *Cell Death Dis.* **2018**, *9*, 343.
(36) Xie, X.; Li, Y.; Zhu, H.; Chen, L.; Chen, D.; Lin, S.; Fan, T. Melittin Inhibits Growth of Human Osteosarcoma 143B Cells through Induction of Apoptosis via Suppressing the Wnt/β-catenin Signaling Pathway. *Anti-Cancer Agents Med. Chem.* **2022**, *22*, 3172−3181.
(37) Kansara, M.; Teng, M. W.; Smyth, M. J.; Thomas, D. M. Translational biology of osteosarcoma. *Nat. Rev. Cancer* **2014**, *14*, 722−735.
(38) Anastas, J. N.; Moon, R. T. WNT signalling pathways as therapeutic targets in cancer. *Nat. Rev. Cancer* **2013**, *13*, 11−26.
(39) Jiang, Y.; Zhang, C.; Lu, L.; Wang, X.; Liu, H.; Jiang, Y.; Hong, L.; Chen, Y.; Huang, H.; Guo, D. The Prognostic Role of Cyclin D1 in Multiple Myeloma: A Systematic Review and Meta-Analysis. *Technol. Cancer Res. Treat* **2022**, *21*, No. 15330338211065252.
(40) Malumbres, M.; Barbacid, M. Cell cycle, CDKs and cancer: a changing paradigm. *Nat. Rev. Cancer* **2009**, *9*, 153−166.
(41) Suski, J. M.; Braun, M.; Strmiska, V.; Sicinski, P. Targeting cell-cycle machinery in cancer. *Cancer Cell* **2021**, *39*, 759−778.
(42) Xia, W.; Lo, C. M.; Poon, R. Y. C.; Cheung, T. T.; Chan, A. C. Y.; Chen, L.; Yang, S.; Tsao, G. S. W.; Wang, X. Q. Smad inhibitor induces CSC differentiation for effective chemosensitization in cyclin D1- and TGF-β/Smad-regulated liver cancer stem cell-like cells. *Oncotarget* **2017**, *8*, 38811−38824.
(43) Donigan, J. M.; De Luca, J.; Lum, C. Cyclin D1 and p16 Expression in Blue Nevi and Malignant Melanoma. *Appl. Immunohistochem. Mol. Morphol.* **2017**, *25*, 91−94.
(44) Wang, Y.; Li, W.; Wang, Z.; Ren, H.; Li, Y.; Zhang, Y.; Yang, P.; Pan, S. Genistein upregulates cyclin D1 and CDK4 expression and promotes the proliferation of ovarian cancer OVCAR-5 cells. *Clin. Chim. Acta* **2021**, *512*, 100−105.
(45) Park, S.; Lim, W.; Bazer, F. W.; Whang, K.-Y.; Song, G. Quercetin inhibits proliferation of endometriosis regulating cyclin D1 and its target microRNAs in vitro and in vivo. *J. Nutr. Biochem.* **2019**, *63*, 87−100.
(46) Ferreira-Silva, G. Á.; Lages, C. C. L.; Sartorelli, P.; Hasegawa, F. R.; Soares, M. G.; Ionta, M. Casearin D inhibits ERK phosphorylation and induces downregulation of cyclin D1 in HepG2 cells. *Toxicol. In Vitro* **2017**, *38*, 27−32.
(47) Fu, L.; Chen, S.; He, G.; Chen, Y.; Liu, B. Targeting Extracellular Signal-Regulated Protein Kinase 1/2 (ERK1/2) in Cancer: An Update on Pharmacological Small-Molecule Inhibitors. *J. Med. Chem.* **2022**, *65*, 13561−13573.
(48) Roberts, P. J.; Der, C. J. Targeting the Raf-MEK-ERK mitogen-activated protein kinase cascade for the treatment of cancer. *Oncogene* **2007**, *26*, 3291−3310.
(49) Gong, C.; Sun, K.; Xiong, H. H.; Sneh, T.; Zhang, J.; Zhou, X.; Yan, P.; Wang, J. H. Expression of CXCR4 and MMP-2 is associated with poor prognosis in patients with osteosarcoma. *Histol. Histopathol.* **2020**, *35*, 863−870.
(50) Fromigué, O.; Hamidouche, Z.; Marie, P. J. Blockade of the RhoA-JNK-c-Jun-MMP2 cascade by atorvastatin reduces osteosarcoma cell invasion. *J. Biol. Chem.* **2008**, *283*, 30549−30556.
(51) Obeng, E. Apoptosis (programmed cell death) and its signals - A review. *Braz. J. Biol.* **2021**, *81*, 1133−1143.
(52) Kumar, P.; Nagarajan, A.; Uchil, P. D. Analysis of Cell Viability by the Lactate Dehydrogenase Assay. *Cold Spring Harb. Protoc.* **2018**, *2018*, No. pdb.prot095497.
(53) Hassan, Y. A.; Helmy, M. W.; Ghoneim, A. I. Combinatorial antitumor effects of amino acids and epigenetic modulations in hepatocellular carcinoma cell lines. *Naunyn-Schmiedeberg's Arch. Pharmacol.* **2021**, *394*, 2245−2257.
(54) Sheen, J. H.; Zoncu, R.; Kim, D.; Sabatini, D. M. Defective regulation of autophagy upon leucine deprivation reveals a targetable liability of human melanoma cells in vitro and in vivo. *Cancer Cell* **2011**, *19*, 613−628.
(55) Lieu, E. L.; Nguyen, T.; Rhyne, S.; Kim, J. Amino acids in cancer. *Exp. Mol. Med.* **2020**, *52*, 15−30.
(56) Rimassa, L.; Danesi, R.; Pressiani, T.; Merle, P. Management of adverse events associated with tyrosine kinase inhibitors: Improving outcomes for patients with hepatocellular carcinoma. *Cancer Treat Rev.* **2019**, *77*, 20−28.
(57) Zhang, H.; Kong, Q.; Wang, J.; Jiang, Y.; Hua, H. Complex roles of cAMP-PKA-CREB signaling in cancer. *Exp. Hematol. Oncol.* **2020**, *9*, 32.
(58) Chin, K. V.; Yang, W. L.; Ravatn, R.; Kita, T.; Reitman, E.; Vettori, D.; Cvijic, M. E.; Shin, M.; Iacono, L. Reinventing the wheel of cyclic AMP: novel mechanisms of cAMP signaling. *Ann. N. Y. Acad. Sci.* **2002**, *968*, 49−64.
(59) Khannpnavar, B.; Mehta, V.; Qi, C.; Korkhov, V. Structure and function of adenylyl cyclases, key enzymes in cellular signaling. *Curr. Opin. Struct. Biol.* **2020**, *63*, 34−41.
(60) Chen, T. C.; Hinton, D. R.; Zidovetzki, R.; Hofman, F. M. Up-regulation of the cAMP/PKA pathway inhibits proliferation, induces differentiation, and leads to apoptosis in malignant gliomas. *Lab. Invest.* **1998**, *78*, 165−174.
(61) Hara, M.; Takeba, Y.; Iiri, T.; Ohta, Y.; Ootaki, M.; Watanabe, M.; Watanabe, D.; Koizumi, S.; Otsubo, T.; Matsumoto, N. Vasoactive intestinal peptide increases apoptosis of hepatocellular carcinoma by inhibiting the cAMP/Bcl-xL pathway. *Cancer Sci.* **2019**, *110*, 235−244.
(62) Brudvik, K. W.; Paulsen, J. E.; Aandahl, E. M.; Roald, B.; Taskén, K. Protein kinase A antagonist inhibits β-catenin nuclear translocation, c-Myc and COX-2 expression and tumor promotion in Apc(Min/+) mice. *Mol. Cancer* **2011**, *10*, 149.
(63) Zhao, Y.; Liao, Q.; Zhu, Y.; Long, H. Endothelin-1 promotes osteosarcoma cell invasion and survival against cisplatin-induced apoptosis. *Clin. Orthop. Relat. Res.* **2011**, *469*, 3190−3199.
(64) Felx, M.; Guyot, M. C.; Isler, M.; Turcotte, R. E.; Doyon, J.; Khatib, A. M.; Leclerc, S.; Moreau, A.; Moldovan, F. Endothelin-1 (ET-1) promotes MMP-2 and MMP-9 induction involving the transcription factor NF-kappaB in human osteosarcoma. *Clin. Sci. (Lond)* **2006**, *110*, 645−654.
(65) Roskoski, R., Jr. The role of small molecule platelet-derived growth factor receptor (PDGFR) inhibitors in the treatment of neoplastic disorders. *Pharmacol. Res.* **2018**, *129*, 65−83.
(66) Osman, I.; Dong, K.; Kang, X.; Yu, L.; Xu, F.; Ahmed, A. S. I.; He, X.; Shen, J.; Hu, G.; Zhang, W.; Zhou, J. YAP1/TEAD1 upregulate platelet-derived growth factor receptor beta to promote vascular smooth muscle cell proliferation and neointima formation. *J. Mol. Cell. Cardiol.* **2021**, *156*, 20−32.
(67) Zhang, Y.; Cedervall, J.; Hamidi, A.; Herre, M.; Viitaniemi, K.; D'Amico, G.; Miao, Z.; Unnithan, R. V. M.; Vaccaro, A.; van Hooren, L.; Georganaki, M.; Thulin, Å.; Qiao, Q.; Andrae, J.; Siegbahn, A.; Heldin, C. H.; Alitalo, K.; Betsholtz, C.; Dimberg, A.; Olsson, A. K. Platelet-Specific PDGFB Ablation Impairs Tumor Vessel Integrity and Promotes Metastasis. *Cancer Res.* **2020**, *80*, 3345−3358.
(68) Thies, K. A.; Hammer, A. M.; Hildreth, B. E., 3rd; Steck, S. A.; Spehar, J. M.; Kladney, R. D.; Geisler, J. A.; Das, M.; Russell, L. O.; Bey, J. F. T.; Bolyard, C. M.; Pilarski, R.; Trimboli, A. J.; Cuitiño, M. C.; Koivisto, C. S.; Stover, D. G.; Schoenfield, L.; Otero, J.; Godbout, J. P.; Chakravarti, A.; Ringel, M. D.; Ramaswamy, B.; Li, Z.; Kaur, B.; Leone, G.; Ostrowski, M. C.; Sizemore, S. T.; Sizemore, G. M. Stromal Platelet-Derived Growth Factor Receptor-β Signaling Promotes Breast Cancer Metastasis in the Brain. *Cancer Res.* **2021**, *81*, 606−618.

https://doi.org/10.1021/acsami.2c21485
ACS Appl. Mater. Interfaces 2023, 15, 26227−26240

(69) Wang, Y.; Mandal, D.; Wang, S.; Kleinerman, E. S.; Pollock, R. E.; Lev, D.; Hayes-Jordan, A. Platelet-derived growth factor receptor beta inhibition increases tumor necrosis factor-related apoptosis-inducing ligand (TRAIL) sensitivity: imatinib and TRAIL dual therapy. *Cancer* **2010**, *116*, 3892−3902.
(70) Motegi, A.; Fujimoto, J.; Kotani, M.; Sakuraba, H.; Yamamoto, T. ALK receptor tyrosine kinase promotes cell growth and neurite outgrowth. *J. Cell Sci.* **2004**, *117*, 3319−3329.
(71) Rajoria, S.; Suriano, R.; Wilson, Y. L.; Schantz, S. P.; Moscatello, A.; Geliebter, J.; Tiwari, R. K. 3,3′-diindolylmethane inhibits migration and invasion of human cancer cells through combined suppression of ERK and AKT pathways. *Oncol. Rep.* **2011**, *25*, 491−497.
(72) Han, J.; Liu, Y.; Yang, S.; Wu, X.; Li, H.; Wang, Q. MEK inhibitors for the treatment of non-small cell lung cancer. *J. Hematol. Oncol.* **2021**, *14*, 1.
(73) Degirmenci, U.; Wang, M.; Hu, J. Targeting Aberrant RAS/RAF/MEK/ERK Signaling for Cancer Therapy. *Cell* **2020**, *9*, 198.
(74) Savoia, P.; Fava, P.; Casoni, F.; Cremona, O. Targeting the ERK Signaling Pathway in Melanoma. *Int. J. Mol. Sci.* **2019**, *20*, 1483.
(75) Routledge, D.; Scholpp, S. Mechanisms of intercellular Wnt transport. *Development* **2019**, *146*, 10.
(76) Zhong, Z. A.; Michalski, M. N.; Stevens, P. D.; Sall, E. A.; Williams, B. O. Regulation of Wnt receptor activity: Implications for therapeutic development in colon cancer. *J. Biol. Chem.* **2021**, *296*, No. 100782.

https://doi.org/10.1021/acsami.2c21485
ACS Appl. Mater. Interfaces 2023, 15, 26227−26240